An Adaptive Aeroelastic Control Approach by using Nonlinear Reduced Order Models

N. D. Tantaroudas *
University of Liverpool, Liverpool, L69 3GH, United Kingdom
A. Da.Ronch †
University of Southampton, Southampton, S017 1BJ, United Kingdom
G. Gai ‡ and K. J. Badcock §
University of Liverpool, Liverpool, L69 3GH, United Kingdom
R. Palacios ¶
Imperial College, London, SW7 2AZ, United Kingdom

A systematic approach to the model order reduction of high fidelity coupled fluid-structure/flight dynamics models and the subsequent control design is described. It uses information on the eigenspectrum of the coupled-system Jacobian matrix and projects the system through a series expansion onto a small basis of eigenvectors representative of the full-model dynamics. A nonlinear reduced order model is derived and is exploited for a worst case gust and adaptive control design. The investigation focuses on a flight control design based on the model reference adaptive control scheme via the Lyapunov stability approach. The novelty of this paper is two-fold. Firstly, it uses a single nonlinear reduced model for parametric worst case gust search. Secondly, it is shown that it makes feasible an implementation of a complex control methodology for a large nonlinear system. The adaptive controller is able to alleviate gust loads for a three degrees-of-freedom aerofoil and for an unmanned aerial vehicle. An investigation for the adaptation parameters is performed and their effect on control input actuation and aeroelastic closed-loop response is discussed.

Nomenclature

b	= semi-chord
K_ξ, K_α, K_δ	= plunge stiffness,torsional and flap stiffness about elastic axis
$K_{\xi 3}$, $K_{\alpha 3}$, $K_{\delta 3}$	= plunge, torsional and flap third order terms of stiffness
$K_{\xi 5}$, $K_{\alpha 5}$, $K_{\delta 5}$	= plunge, torsional and flap fifth order terms of stiffness
I_α	= second moment of inertia of aerofoil about elastic axis
I_δ	= flap moment of inertia
m	= aerofoil sectional mass
h	= plunge displacement
k	= reduced oscillation frequency, $\omega\, c\,/\,2\, U_\infty$
t	= physical time
x_α	= aerofoil static unbalance, $S_\alpha / m\, b$
x_δ	= reduced centre of gravity distance from flap hinge.

*Ph.D. Student, School of Engineering; ntanta@liverpool.ac.uk (Corresponding Author).
†Lecturer, Faculty of Engineering and the Environment; Member AIAA.
‡PhD. Student, School of Engineering.
§Professor, School of Engineering. Senior Member AIAA.
¶Reader, Department of Aeronautics. Member AIAA.

$\boldsymbol{R}$ = residual vector
c_h = non-dimensional distance from the mid-chord to the flap hinge
r_a = radius of gyration of aerofoil about elastic axis, $r_a^2 = I_\alpha / m\, b^2$
r_δ = reduced radius of flap gyration
U_∞ = freestream velocity
U_L = linear flutter speed
U^* = reduced velocity, $U/b\,\omega_\alpha$
$\boldsymbol{w}$ = vector of unknowns
$\boldsymbol{A}, \boldsymbol{B}, \boldsymbol{C}$ = first,second and third order Jacobian operators
$\boldsymbol{B}_c, \boldsymbol{B}_w$ = control,and disturbance recuded vector
$\boldsymbol{A}_m, \boldsymbol{B}_m$ = jacobian and control input vector of the reference model
w_g = gust vertical normalized velocity
W_0 = intensity of gust vertical velocity

Greek

α = angle of attack
δ = trailing-edge flap deflection
τ = non-dimensional time, $t\,U_\infty\,/\,b$
ω_ξ = uncoupled plunging mode natural frequency, $\sqrt{K_\xi/m}$
ω_α = uncoupled pitching mode natural frequency about elastic axis, $\sqrt{K_\alpha/I_\alpha}$
ω_δ = uncoupled flapping mode natural frequency $\sqrt{K_\delta}/I_\delta$
$\bar{\omega_1}$ = ratio of ω_ξ/ω_α
$\bar{\omega_2}$ = ratio of $\omega_\delta/\omega_\alpha$
ζ_ξ = damping ratio in plunge, C_ξ/C_ξ^c
ζ_α = damping ratio in pitch, C_α/C_α^c
ζ_δ = damping ratio in flap, $C_\delta/2\sqrt{I_\delta K_\delta}$
ξ = non-dimensional displacement in plunge, h/b
μ = mass ratio, $m/\pi\,\rho\,b^2$
Φ = matrix of right coupled system eigenvectors

I. Introduction

The following investigation focuses and builds on previous work done on the development of a systematic approach to flight control system (FCS) design for very flexible or very large aircraft.[1–4] In this paper, the focus is on the exploitation of model order reduction for gust load alleviation by an adaptive control implementation. Previous work by the authors has focused on gust load prediction and alleviation using standard robust optimal control techniques based on H_∞ and H_2.[3,5] Recent work [4] has dealt with flutter suppression by means of active control and use of control surfaces for an experimental wind tunnel model. The role of reduced order models was also investigated.

A large body of work has been done in linear control design for nonlinear aeroelastic systems and even though linear controllers can most times stabilize a nonlinear system around a stable controllable equilibrium, stability is not guaranteed under strong nonlinear regimes. Thus, several studies focused on eliminating the nonlinearity that induced pathologies such as limit cycle oscillations based on partial feedback linearisation control.[6] The nonlinear active control designed by Strganac et al[6] required that the controller needed a well known nonlinearity for the exact cancelation. As a continuation of this work, the authors of this investigation performed partial feedback linearization for a numerical model corresponding to a low speed wind tunnel model with a nonlinearity in the plunge degree of freedom.[7] It was shown that the nonlinear controller outperforms a linear control design based on pole placement as the latter fails to achieve any significant reduction in the amplitude of the LCO. Also, optimal control has been tested for flutter suppression, for example, Huang et al [8] designed a Linear Quadratic Gaussian control that takes into account a control input delay and applied the control at an experimental wind tunnel model for flutter suppression. Aside from flutter suppression significant amount of effort for control design has been shown for stability augmentation

and gust load alleviation in flexible aircraft.[9,10] A common approach is to fully account for the nonlinear structural behaviour while simple linear aerodynamic models based on two-dimensional theory were used for the aerodynamics.

In general, common linear control methodologies have been found efficient for aeroelastic systems at a specific freestream speed region but ideally as the flow conditions during flight may change, an adaptive control methodology is preferred. Recent advances in adaptive control and especially in L_1 adaptive control theory made possible the application of adaptive controllers to the control of uncertain nonlinear systems.[11] This design uses a state predictor similar to indirect model reference adaptive systems however the control input is obtained by filtering the estimated control signal with a low pass filter. L_1 adaptive approach has been applied to the wing-rock control[12] and missile control.[13] In Ref.[14] an L_1 adaptive controller for a prototypical pitch-plunge 2-D aeroelastic system in the presence of gust loads was developed. Other techniques of adaptive control such as model reference adaptive control have been applied at a flexible aircraft problem by using a rigid aircraft as a reference model and a neural network adaptation to control the structural flexible modes and compensate for the effects of unmodeled dynamics.[15] Recently Chowdhary et al.[16] presented flight tests results for adaptive controllers based on the Model Reference Adaptive Control (MRAC) architecture on the Georgia Tech GT Twinstar fixed wing engine aircraft with 25% of the wing missing. A recent promising adaptive control architecture was based on the derivative free MRAC[17] method. This new algorythm is expected to provide faster adaptation and smoother error transients particularly for situations where the system dynamics are changing fast.

The paper continues in § II with a description of the full order model. The approach to model reduction and the control design is introduced in § III and in § IV, respectively. Finally, validation of the code against existing numerical and published data, a worst-case gust search and the application of the controller for load alleviation for a 3 degrees-of-freedom and an unmanned aerial vehicle are presented.

II. Full Order Model

The general form of the fully coupled nonlinear model for the description of the flight dynamics of a very flexible aircraft can be represented in state-space form. Denote by $\boldsymbol{w}$ the n-dimensional state-space vector which is conveniently partitioned into fluid, structural and rigid body degrees of freedom.

$$\boldsymbol{w} = \left(\boldsymbol{w}_f^T, \boldsymbol{w}_s^T, \boldsymbol{w}_r^T\right) \tag{1}$$

The state-space equations in the general vector form are

$$\frac{d\boldsymbol{w}}{dt} = \boldsymbol{R}\left(\boldsymbol{w}, \boldsymbol{u}_c, \boldsymbol{u}_d\right) \tag{2}$$

where $\boldsymbol{R}$ is the nonlinear residual, $\boldsymbol{u}_c$ is the input vector (e.g. control flap deflections or thrust) and $\boldsymbol{u}_d$ is the exogenous vector for the description of some form of disturbance acting on the system (e.g. gust). The homogeneous system has an equilibrium point, $\boldsymbol{w}_0$, for given constant $\boldsymbol{u}_{c0}$ and $\boldsymbol{u}_{d0} = 0$ corresponding to a constant solution in the state-space and satisfying

$$\frac{d\boldsymbol{w}_0}{dt} = \boldsymbol{R}\left(\boldsymbol{w}_0, \boldsymbol{u}_{c0}, \boldsymbol{u}_{d0}\right) = 0 \tag{3}$$

The residual form in Eq. (3) forms the reference for the model reduction described below. The system is often parametrized in terms of an independent parameter (freestream-speed, air density, altitude, etc.) for stability analysis. The options for the residual evaluation are described in the next section.

A. Linear Aerodynamic Model

A cheaper computational alternative to the computational fluid dynamics (CFD) valid for an irrotational and incompressible two-dimensional flow is the aerodynamic model given by the classical theory of Theodorsen.[18] This is a reasonable assumption when dealing with low-speed flow characteristics in 2-D. The total unsteady aerodynamic forces and moments can be separated into three components, circulatory, non-circulatory due to the wing motion and a contribution from the gust disturbance. The aerodynamic loads due to an arbitrary input time-history are obtained through convolution against a kernel function. For the influence of aerofoil motion on the loads, the Wagner function is used.[19] In a similar way, the influence of the gust is performed

by introducing the Küssner function.[20] Since the assumption is of linear aerodynamics, the effects of both influences are added together to find the variation of the forces and moments for a given motion and gust. For a practical evaluation of the integral, a two lag exponential approximation is used for the Wagner and Küssner functions.

B. Residual Formulation

The residual formulation for the two testcases investigated here follows the general formulation of the full order model as described in II. Both testcases include a nonlinear structural model. The 3 degrees of freedom aerofoil model, can have a cubic or quintic structural polynomial stiffness nonlinearity in any of the structural degrees of freedom while the beam model is based on an exact geometric nonlinearity.

1. *Three Degree-of-Freedom Model*

The size of the coupled aeroelastic model is 14 and consists of 8 aerodynamic states and 6 structural states (pitch, plunge and flap degrees-of-freedom and their corresponding velocities) . The nondimensional torque is used as control input related to the flap rotation. Define the state vector $\boldsymbol{x_s}$ of the structural degrees-of-freedom and $\boldsymbol{w_f}$ for the augmented aerodynamic states.

$$\boldsymbol{x_s} = (\xi, \alpha, \delta)^T \tag{4}$$

$$\boldsymbol{w_f} = (w_1, w_2, w_3, w_4, w_5, w_6, w_7, w_8) \tag{5}$$

Following the general definition of the Residual in § II the system is recast in a coupled first order ODE of the general form where the unknowns are partitioned into structural and fluid contribution as

$$\boldsymbol{w} = \left(\boldsymbol{w}_s^T, \boldsymbol{w}_f^T\right)^T \quad \text{where} \quad \boldsymbol{w}_s = \left(\boldsymbol{x}_s^T, \dot{\boldsymbol{x}}_s^T\right)^T \tag{6}$$

and the residual $\boldsymbol{R}$ is given by

$$\boldsymbol{R} = \boldsymbol{A}_L\boldsymbol{w} + \boldsymbol{b}_N(\boldsymbol{w}) + \boldsymbol{b}_a + \boldsymbol{b}_e \tag{7}$$

The matrix A_L is defined as

$$\boldsymbol{A}_L = \begin{bmatrix} \boldsymbol{0} & \boldsymbol{I} & \boldsymbol{0} \\ -\boldsymbol{M}^{-1}\boldsymbol{K} & -\boldsymbol{M}^{-1}\boldsymbol{C} & \boldsymbol{A}_{sf} \\ \boldsymbol{A}_{fs} & \boldsymbol{0} & \boldsymbol{A}_{ff} \end{bmatrix} \tag{8}$$

$$\boldsymbol{b}_N = \begin{Bmatrix} \boldsymbol{0} \\ -\boldsymbol{M}^{-1}\boldsymbol{F}_N \\ \boldsymbol{0} \end{Bmatrix}, \quad \boldsymbol{b}_a = \begin{Bmatrix} \boldsymbol{0} \\ -\boldsymbol{M}^{-1}\boldsymbol{f}_a \\ \boldsymbol{0} \end{Bmatrix}, \quad \boldsymbol{b}_e = \begin{Bmatrix} \boldsymbol{0} \\ -\boldsymbol{M}^{-1}\boldsymbol{f}_e \\ \boldsymbol{A}_{fg}\boldsymbol{u}_d \end{Bmatrix} \tag{9}$$

The matrix terms $\boldsymbol{M}$, $\boldsymbol{C}$ and $\boldsymbol{K}$ are the effective mass, damping and stiffness matrices containing structural and aerodynamic contributions. The matrix blocks $\boldsymbol{A}_{sf}$ and $\boldsymbol{A}_{fs}$ couple the structural equations and the fluid equations. The matrix $\boldsymbol{A}_{ff}$ relates the fluid unknowns to their first time derivatives. The term $\boldsymbol{F}_N$ is a nonlinear vector arising from the polynomial stiffness. The vector $\boldsymbol{f}_a$ arises from the influence of initial conditions upon the unsteady aerodynamic forces. The term $\boldsymbol{f}_e$ is the nondimensionalised form of any applied external force or moment, for e.g. the flap hinge moment for control input. Overall, vectors $\boldsymbol{b}_N$, $\boldsymbol{b}_a$ and $\boldsymbol{b}_e$ denote contributions from nonlinear terms, aerodynamics due to initial conditions and external inputs, respectively.

2. *Geometrically-Nonlinear Flexible Wing*

The stuctural dynamic description based on the geometrically-exact nonlinear beam equations detailed in [21] is used for the structural model and a thin-strip theory is used for the unsteady aerodynamics. The coupled full order model follows the formulation presented in.[1] Results are obtained using two-noded displacement-based elements. In a displacement-based formulation, dominant nonlinearities arising from large deformations are cubic terms, as opposed to an intrinsic description where they appear up to second order.[22] The nonlinear beam code was coupled with strip aerodynamics using the description above. The motion of each structural

node is described by 6 degrees-of-freedom. The coupling between aerodynamic and structural models is performed considering that each structural node coincides with an aerodynamic section. No aeroelastic interface is required in this case, as the aerodynamic forces and moments are applied directly on each structural node. For cases where an aeroelastic interface is required to couple non-coincident and non-overlapping aerodynamic/structural models, the method described in Ref.[23] provides an excellent solution to the problem.

Similarly, the system is recast in a coupled first order ODE of the general form as in Eq. (2)

$$\boldsymbol{R} = \boldsymbol{A}\boldsymbol{w} + \boldsymbol{B}_c\boldsymbol{u}_c + \boldsymbol{B}_g\boldsymbol{u}_d + \boldsymbol{F}_N(\boldsymbol{w}) \tag{10}$$

where the unknowns are partitioned into structural and fluid contribution as Eq. (6)

$$\boldsymbol{w} = \left(\boldsymbol{w}_s^T, \boldsymbol{w}_f^T\right)^T \quad \text{where} \quad \boldsymbol{w}_s = \left(\boldsymbol{x}_s^T, \dot{\boldsymbol{x}}_s^T\right)^T \tag{11}$$

The matrix $\boldsymbol{A}$ is defined as,

$$\boldsymbol{A} = \begin{bmatrix} \boldsymbol{0} & \boldsymbol{I} & \boldsymbol{0} \\ -\boldsymbol{M}_T^{-1}\boldsymbol{K}_T & -\boldsymbol{M}_T^{-1}\boldsymbol{C}_T & \boldsymbol{A}_{sf} \\ \boldsymbol{A}_{fs} & \boldsymbol{0} & \boldsymbol{A}_{ff} \end{bmatrix} \tag{12}$$

while the contributions from gust and control rotation are given in Eq. (13) respectively.

$$\boldsymbol{B}_c = \begin{Bmatrix} \boldsymbol{0} \\ \boldsymbol{M}_T^{-1}\boldsymbol{A}_{sc} \\ \boldsymbol{A}_{fc} \end{Bmatrix}, \qquad \boldsymbol{B}_g = \begin{Bmatrix} \boldsymbol{0} \\ \boldsymbol{0} \\ \boldsymbol{A}_{fg} \end{Bmatrix} \tag{13}$$

Lastly the structural nonlinearities are assembled in the vector $\boldsymbol{F}_N$ forming the nonlinear residual. Note that Eq. (10) has the same structure that Eq. (7) has, even though they were derived from different modelling techniques.

III. Nonlinear Model Reduction

Denote $\Delta\boldsymbol{w} = \boldsymbol{w} - \boldsymbol{w}_0$ the increment in the state-space vector with respect to an equilibrium solution. The large-order nonlinear residual is expanded in a Taylor series around the equilibrium point

$$\boldsymbol{R}(\boldsymbol{w}) \approx \boldsymbol{A}\,\Delta\boldsymbol{w} + \frac{\partial\boldsymbol{R}}{\partial\boldsymbol{u}_c}\Delta\boldsymbol{u}_c + \frac{\partial\boldsymbol{R}}{\partial\boldsymbol{u}_d}\Delta\boldsymbol{u}_d + \frac{1}{2}\boldsymbol{B}(\Delta\boldsymbol{w}, \Delta\boldsymbol{w}) + \frac{1}{6}\boldsymbol{C}(\Delta\boldsymbol{w}, \Delta\boldsymbol{w}, \Delta\boldsymbol{w}) + \mathcal{O}\left(|\Delta\boldsymbol{w}|^4\right) \tag{14}$$

retaining terms up to third order in the perturbation variable to describe the nonlinear full order dynamics. The Jacobian matrix of the system is denoted as $\boldsymbol{A}$ and the vectors $\boldsymbol{B}$ and $\boldsymbol{C}$ indicate, respectively, the second and third order Jacobian operators. The control surface deflection and gust disturbance is indicated by $\boldsymbol{u}_c$ and $\boldsymbol{u}_d$, respectively.

$$\boldsymbol{A}\,\boldsymbol{x} = \frac{\boldsymbol{R}_1 - \boldsymbol{R}_{-1}}{2\,\epsilon} \tag{15}$$

$$\boldsymbol{B}(\boldsymbol{x}, \boldsymbol{x}) = \frac{\boldsymbol{R}_1 - 2\,\boldsymbol{R}_0 + \boldsymbol{R}_{-1}}{\epsilon^2} \tag{16}$$

$$\boldsymbol{C}(\boldsymbol{x}, \boldsymbol{x}, \boldsymbol{x}) = \frac{-\boldsymbol{R}_3 + 8\,\boldsymbol{R}_2 - 13\,\boldsymbol{R}_1 + 13\,\boldsymbol{R}_{-1} - 8\,\boldsymbol{R}_{-2} + \boldsymbol{R}_{-3}}{8\,\epsilon^3} \tag{17}$$

where $\boldsymbol{R}_l = \boldsymbol{R}(\boldsymbol{x}_0 + l\,\epsilon\,\Delta\boldsymbol{x})$.

The full order system is projected onto a basis formed by a small number of eigenvectors of the Jacobian matrix evaluated at the equilibrium position. Right and left eigenvectors are scaled to satisfy the biorthonormality condition.[1] The projection of the full order model is done using a transformation of coordinates

$$\Delta w = \Phi\,z + \bar{\Phi}\,\bar{z} \tag{18}$$

where z is the state space vector governing the dynamics of the reduced order system and Φ is the modal matrix of right coupled system eigenvectors. The result is a system of uncoupled ordinary differential equations in z. The dependencies of the residual on control surface deflection and gust are evaluated by

finite differences. A clear choice for the basis is to use eigenvectors corresponding to structural modeshapes modified by the flow at the specific equilibrium point, which are readily available when tracking frequencies and modeshapes for increasing air speed. This is equivalent to adding aerodynamic mass, damping and inertia. If required, the basis can be enhanced by including additional eigenvectors until convergence.

The advantages of the approach are that: 1) it can retain non–linear effects from the original full order model; 2) once created, it is independent of the gust formulation and one reduced model can be used for parametric searches; 3) it allows control design on a small non–linear system and offers the possibility to investigate non–linear control techniques; and 4) the approach is systematic because control design is done in the same way independently of the formulation of the full order model. This technique only requires a coupled system in first order form.

IV. Model Reference Adaptive Control

This section describes how linear and nonlinear reduced models are used to design control laws based on model reference adaptive control. The stability proof of this methodology is well known.[24] This approach assumes an ideal reference model which will induce some constraints on the response of the actual aeroelastic system. The dynamics of the reduced model are given by Eq. (19)

$$\boldsymbol{x}\left(t\right)' \;=\; \boldsymbol{A}\,\boldsymbol{x}\left(t\right) \;+\; \boldsymbol{B}_c\,\boldsymbol{u}_c\left(t\right) + \boldsymbol{B}_g\boldsymbol{u}_d\left(t\right) \;+\; \boldsymbol{F}_{NR}\left(\boldsymbol{x}\right) \tag{19}$$

where $\boldsymbol{F}_{NR}$ is the nonlinearity that results from the nonlinear model order reduction technique. The assumed ideal model reference follows dynamics of the form

$$\boldsymbol{x}_m\left(t\right)' \;=\; \boldsymbol{A}_m\,\boldsymbol{x}_m\left(t\right) \;+\; \boldsymbol{B}_m\,\boldsymbol{u}_c\left(t\right) \;+\; \boldsymbol{B}_g\boldsymbol{u}_d\left(t\right) \;+\; \boldsymbol{F}_{NR}\left(\boldsymbol{x}_m\right) \tag{20}$$

The nonlinearity in the reference model has been selected to satisfy $\boldsymbol{F}_{NR}\left(\boldsymbol{x}\right) = \boldsymbol{F}_{NR}\left(\boldsymbol{x}_m\right) = \boldsymbol{F}_{NR}$. Matrix $\boldsymbol{A}_m$ is a stable Hurwitz matrix that satisfies the desired properties of the reference system. This could mean eigenvalues with increased damping compared to the actual aeroelastic system. Matrix $\boldsymbol{B}_m$ is user defined and describes the influence of the control inputs on the states of the reference model. The states of the reference model due to the increased damping in matrix $\boldsymbol{A}_m$ will decay to zero faster under the same disturbances or flap actuation while their magnitude will be smaller as well. The physical displacements of the system can be retrieved by using the eigenvectors.

$$\begin{aligned} y\left(t\right) \;&=\; C\boldsymbol{x}\left(t\right) \\ y_m\left(t\right) \;&=\; C\boldsymbol{x}_m\left(t\right) \end{aligned} \tag{21}$$

The goal is to find a dynamic control input $\boldsymbol{u}_c\left(t\right)$ such that $\lim_{t\to\infty}\left\|y\left(t\right) - y_m\left(t\right)\right\|$. The exact control feedback for the model matching conditions is defined as

$$\boldsymbol{u}_c\left(t\right) \;=\; \boldsymbol{K}_x^*\boldsymbol{x}\left(t\right) \;+\; \boldsymbol{K}_r^* r\left(t\right) \tag{22}$$

where $\boldsymbol{r}\left(t\right)$ is a reference signal applied in both systems as shown in Fig. 1 (e.g. torque for the aerofoil model or flap angle for the flexible wing case) and $\boldsymbol{K}_x^*, \boldsymbol{K}_r^*$ are the exact gains acting on the states and control input to match the two models. By replacing Eq. (22) in Eq. (19) and satisfying the model matching conditions yields

$$\begin{aligned} \boldsymbol{A} \;+\; \boldsymbol{B}_c\boldsymbol{K}_x^* &= \boldsymbol{A}_m \\ \boldsymbol{B}_c\boldsymbol{K}_r^* \qquad &= \boldsymbol{B}_m \end{aligned} \tag{23}$$

Since $\boldsymbol{A}$ and $\boldsymbol{B}_c$ are considered to be unknown to the controller the values denoted in Eq. (22) (e.g $\boldsymbol{K}_x^*, \boldsymbol{K}_r^*$) are also unknown at initial time and the actual control signal applied at the current timestep is defined as

$$\boldsymbol{u}_c\left(t\right) \;=\; \boldsymbol{K}_x\left(t\right)\boldsymbol{x}\left(t\right) \;+\; \boldsymbol{K}_r\left(t\right)\boldsymbol{r}\left(t\right) \tag{24}$$

The gains $\boldsymbol{K}_x\left(t\right)$ and $\boldsymbol{K}_r\left(t\right)$ in Eq.(24) are dynamic gains that need to be solved and at the end will be required to converge to the values that provide a solution to Eq. (23). The closed loop dynamics of the nonlinear reduced model at this point can be expressed as

$$\boldsymbol{x}\left(t\right)' \;=\; \left(\boldsymbol{A} \;+\; \boldsymbol{B}_c\boldsymbol{K}_x\left(t\right)\right)\boldsymbol{x}\left(t\right) \;+\; \boldsymbol{B}_c\boldsymbol{K}_r\left(t\right)\boldsymbol{r}\left(t\right) \;+\; \boldsymbol{B}_g\boldsymbol{u}_d\left(t\right) \;+\; \boldsymbol{F}_{NR} \tag{25}$$

Let $\theta^* = [\boldsymbol{K}_x^* \;\; \boldsymbol{K}_r^*]^T$ and $\theta = [\boldsymbol{K}_x(t) \;\; \boldsymbol{K}_r(t)]^T$. The estimation error between the instantaneous and the ideal gains is defined as

$$\bar{\theta} = \theta^* - \theta = \left(\bar{\theta}_x \;\; \bar{\theta}_r\right)^T \tag{26}$$

with $\bar{\theta}_x = \boldsymbol{K}_x^* - \boldsymbol{K}_x(t)$, $\bar{\theta}_r = \boldsymbol{K}_r^* - \boldsymbol{K}_r(t)$. Now define $\phi = \left(\boldsymbol{x}(t)^T \;\; \boldsymbol{r}(t)\right)^T$. In that case the closed loop system dynamics in Eq. (25) are expressed as

$$\begin{aligned}\boldsymbol{x}(t)' &= (\boldsymbol{A} + \boldsymbol{B}_c\boldsymbol{K}_x^*)\boldsymbol{x}(t) + \boldsymbol{B}_c\boldsymbol{K}_r^*\boldsymbol{r}(t) - \boldsymbol{B}_c\bar{\theta}_x\boldsymbol{x}(t) - \boldsymbol{B}_c\bar{\theta}_r\boldsymbol{r}(t) + \boldsymbol{B}_g\boldsymbol{u}_d(t) + \boldsymbol{F}_{NR} \\ &= \boldsymbol{A}_m\boldsymbol{x}(t) + \boldsymbol{B}_m\boldsymbol{r}(t) - \boldsymbol{B}_c\phi^T\bar{\theta} + \boldsymbol{B}_g\boldsymbol{u}_d(t) + \boldsymbol{F}_{NR}\end{aligned} \tag{27}$$

For the purpose of the stability proof of the closed loop system one needs to define the error dynamics between the two systems.

$$\boldsymbol{e}(t) = \boldsymbol{x}(t) - \boldsymbol{x}_m(t) \tag{28}$$

The derivative of which, expresses the rate of change between the two systems and can be written as

$$\begin{aligned}\boldsymbol{e}(t)' &= \boldsymbol{x}(t)' - \boldsymbol{x}_m(t)' \\ &= \boldsymbol{A}_m\boldsymbol{x}(t) + \boldsymbol{B}_m\boldsymbol{r}(t) - \boldsymbol{B}_c\phi^T\bar{\theta} + \boldsymbol{F}_{NR} - \boldsymbol{A}_m\boldsymbol{x}_m(t) - \boldsymbol{B}_m\boldsymbol{r}(t) - \boldsymbol{F}_{NR} + \boldsymbol{B}_g\boldsymbol{u}_d(t) - \boldsymbol{B}_g\boldsymbol{u}_d(t) \\ &= \boldsymbol{A}_m(\boldsymbol{x}(t) - \boldsymbol{x}_m(t)) - \boldsymbol{B}_c\phi^T\bar{\theta} \\ &= \boldsymbol{A}_m\boldsymbol{e}(t) - \boldsymbol{B}_c\phi^T\bar{\theta}\end{aligned} \tag{29}$$

The Lyapunov equation is solved for the reference model and its solution will be part of the steady part of the Lyapunov candidate function that will lead to the stability proof of the nonlinear reduced model.

$$\boldsymbol{P}\boldsymbol{A}_m + \boldsymbol{A}_m{}^T\boldsymbol{P} = -\boldsymbol{Q}, \qquad \boldsymbol{Q} = \boldsymbol{Q}^T \geq 0 \tag{30}$$

where in Eq.(30) $\boldsymbol{Q}$ is a semi-definite positive user defined matrix. A scalar quadratic Lyapunov function $\boldsymbol{V}$ in $\boldsymbol{e}$ and $\bar{\theta}$ may be defined, such that the system becomes asymptotically stable by satisfying $\boldsymbol{V} > 0$ and its time derivative is semi definite negative $\boldsymbol{V}' \leq 0$ [24] . This function will provide insight on the selection of the parameter update law of the time varying gains in Eq. (24). The Lyapunov function

$$\boldsymbol{V}(\boldsymbol{e}(t), \theta) = \boldsymbol{e}(t)^T\boldsymbol{P}\boldsymbol{e}(t) + \bar{\theta}^T\boldsymbol{\Gamma}^{-1}\bar{\theta} > 0 \tag{31}$$

is considered, where $\boldsymbol{P} = \boldsymbol{P}^T > 0$ is the solution of the algebraic Lyapunov Eq. (30) for a particular selection of $\boldsymbol{Q}$ while $\boldsymbol{\Gamma} = \boldsymbol{\Gamma}^T \geq 0$ is a user defined semi definite positive matrix. Note that the positiveness of the above Lyapunov function is guaranteed only if the system under examination is a minimum-phase system. Differentiating the above equation with respect to time yields

$$\boldsymbol{V}'(\boldsymbol{e}(t), \theta) = \boldsymbol{e}(t)'^T\left(\boldsymbol{P} + \boldsymbol{P}^T\right)\boldsymbol{e}(t) + 2\bar{\theta}^T\boldsymbol{\Gamma}^{-1}\bar{\theta}' \tag{32}$$

By substitution of the error dynamics and by using Eq. (30) , Eq. (32) is expanded as follows

$$\begin{aligned}\boldsymbol{V}'(\boldsymbol{e}(t), \theta) &= \boldsymbol{e}(t)^T\left(\boldsymbol{A}_m\boldsymbol{P} + \boldsymbol{A}_m{}^TP\right)\boldsymbol{e}(t) + 2\boldsymbol{e}(t)^T\boldsymbol{P}\boldsymbol{B}_c\phi^T\bar{\theta} + 2\bar{\theta}^T\boldsymbol{\Gamma}^{-1}\bar{\theta}' \\ &= -\boldsymbol{e}(t)^T\boldsymbol{Q}\boldsymbol{e}(t) + 2\bar{\theta}^T\boldsymbol{\Gamma}^{-1}\left(\boldsymbol{\Gamma}\phi\boldsymbol{e}(t)^T\boldsymbol{P}\boldsymbol{B}_c + \bar{\theta}'\right)\end{aligned} \tag{33}$$

From the above equation one can determine the adaptation parameter to satisfy the semi definite negativeness of the derivative of the Lyapunov function as

$$\bar{\theta}' = -\boldsymbol{\Gamma}\phi\boldsymbol{e}(t)^T\boldsymbol{P}\boldsymbol{B}_c \tag{34}$$

which leads to

$$\boldsymbol{V}'(\boldsymbol{e}(t), \theta) = -\boldsymbol{e}(t)^T\boldsymbol{Q}\boldsymbol{e}(t) \leq 0 \tag{35}$$

which is valid due to the semi definite positiveness of matrix $\boldsymbol{Q}$. The dynamic time varying gains in Eq. (24) are updated by the adaptive law so that the time derivative of the Lyapunov function decreases along the

error dynamic trajectories as in Eq. (35). By using Barbalat's lemma this translates in boundness of the error dynamics with respect to the time evolution and as a result satisfaction of the model matching conditions. In general, this control approach is limited to minimum phase systems. Thus, when applied in unstable nonminimum phase systems unstable zero-pole cancelation may occur and the error between the two assumed models slowly diverges to infinity. However, a simple feedback based on the Bass-Gura formula [25] can be applied on the ROM to place any unstable zeros on the left half plane. The implementation of the computational algorythm can be summarized in the block diagram shown in Fig. 1.

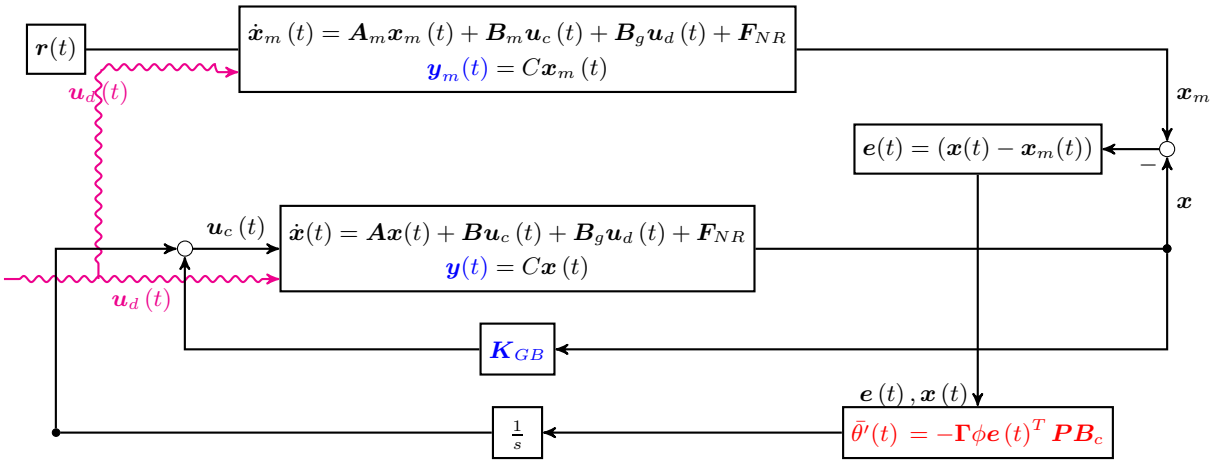

Figure 1. Adaptive Control Algorythm

V. Results

A three degrees-of-freedom aerofoil model and the Global Hawk-like flexible aircraft are the testcases. Results in both cases start from validation, reduced order model generation for worst case gust searches and adaptive gust load alleviation.

A. Three Degrees-of-Freedom Aerofoil

1. *Validation*

Two sets of parameters are considered (see Table 1) and are defined in the nomenclature. The two testcases differ in the ratio of the uncoupled plunging to pitching mode $\overline{\omega}_1$ and c_h which is the non-dimensional distance from the mid-chord to the flap hinge.

Case	$\overline{\omega}_1$	$\overline{\omega}_2$	μ	a_h	x_α	x_δ	r_α	r_δ	c_h
1	0.2	300	100.0	-0.5	0.25	0.0125	0.5	0.0791	0.5
2	1.2	3.5	100.0	-0.5	0.25	0.0125	0.5	0.0791	0.6

Table 1. Model parameters for aerofoil test cases

Linear stability analysis provides a convenient way to verify the linear part of the aerofoil model. Tracing of the structural eigenvalues against the system parameter, the reduced velocity in this case, are most commonly found in available literature. In the following results, the Schur complement form of the eigenvalue problem presented by Badcock and Woodgate[26] is used to track the migration of the three structural eigenvalues with the reduced velocity. The first comparison is made with a two degree-of-freedom (DoF) aerofoil model presented by Alighanbari and Price[27] as well as the original two degree-of-freedom model

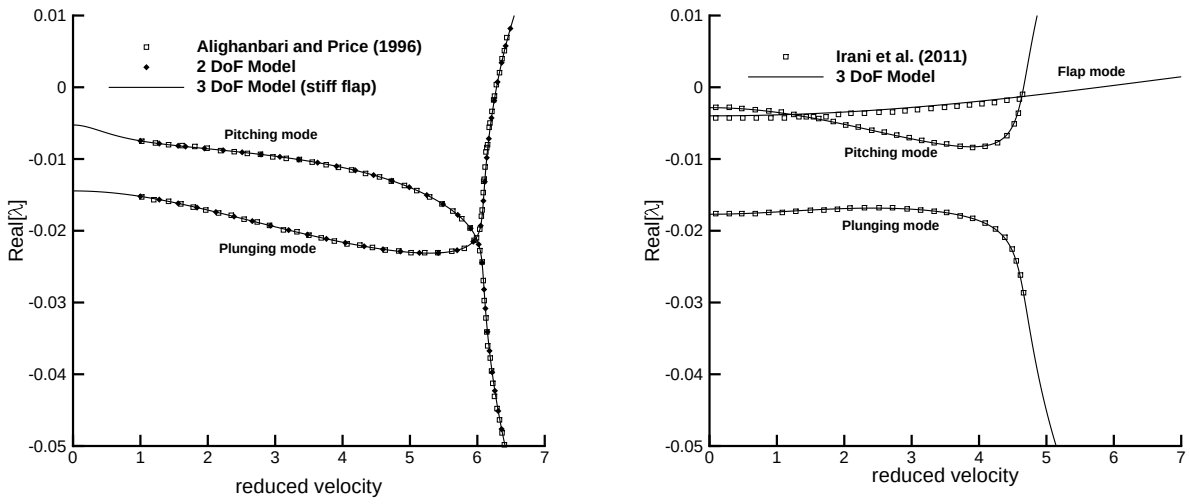

(a) mode trace for case 1

(b) mode trace for case 2

Figure 2. Mode traces for validation test cases 1 and 2

by Da Ronch et al.[28] Since this specific comparison is made between a three degree-of-freedom and a two degree-of-freedom model, it is necessary to enforce a very high stiffness in the flap degree of freedom by setting a high value of $\overline{\omega}_2$. This effectively limits the dynamics of the three degree-of-freedom model to a two degree-of-freedom system. The system parameters used are given in Table 1 for Case 1 with $\overline{\omega}_2$ enforced to be 300. The nonlinear stiffness coefficients are all set to zero. The mode tracing show excellent agreement with the result presented by Alighanbari and Price[27] in Fig. 2 (a). The linear instability point is found to be $U^* = 6.285$.

The flutter speed is also validated against the results presented by Irani et al.[29] The model presented by Irani et al.[29] is a three degree-of-freedom aerofoil and the aeroelastic parameters are directly taken from the paper and given in Table 1 for Case 2. The flutter speed is calculated to be $U^* = 4.663$ which matches the reported value. Figure 2(b) shows the corresponding mode trace comparison. In the aerofoil case the nonlinearity is a polynomial cubic nonlinearity in either the pitch or the plunge degree-of-freedom stiffness and is fully deterministic. So the most important part of the verification is the linear stability analysis presented.

2. Nonlinear Reduced Models for Worst Case Gust Search

Two families of atmospheric gusts are used in this paper, discrete and continuous. The discrete model for the "1-minus-cosine" gust is formulated as

$$W_g(\tau) = \frac{W_0}{2} cos\left(\frac{2\pi}{H_g}(\tau - \tau_0)\right) \tag{36}$$

where W_0 is the gust intensity normalized by the freestream speed and H_g is the gust length. For the generation of continuous models of atmospheric Von Kármán turbulence, the rational approximation documented in [30] can be used. A cubic hardening nonlinearity is considered for the pitch degree-of-freedom $K_{\alpha 3} = 3$ and in the plunge degree-of-freedom $K_{\xi 3} = 1.0$. The aeroelastic nondimensional model parameters given are the same as Case 2 in Table 1 with the difference that now is $\overline{\omega}_1 = 0.2$.

From the bifurcation method and the eigenvalue solution of the linearized system, the instability for this model selection occurs for $U^* = 6.37$. Reduced order models are generated by including the three complex eigenvalues corresponding to the structural degrees-of-freedom and one additional eigenvalue related to the gust influence as shown in Table. 2. The reduced model is used to perform a worst case gust search for the "1-minus-cosine" family. The gust intensity is 14% of the freestream speed at $U^* = 4.5$ or 70.64% or the linear predicted flutter speed, and the search is made for gust lengths up to 100 aerofoil semi-chords.

The parameter space is divided into 1000 design sites. The worst case gust was found to be for $H_g = 55$ semichords corresponding to maximum loads in the pitching angle. Fig. 3 shows the maximum and minimum aeroelastic amplitude for full nonlinear and reduced model against different gust lengths. NFOM denotes nonlinear full order model and NROM denotes nonlinear reduced order model dynamic response. As shown, the nonlinear reduced model can efficiently predict aeroelastic responses if the three complex eigenvalues related to the structural degrees-of-freedom together with one real eigenvalue related to the gust are included in the projection basis. The effect of the nonlinearity in the systems dynamics becomes important and is more evident under larger loads for the worst gust case. The full nonlinear aeroelastic response against the linear and their reduced models in that worst case gust is given in Fig. 4

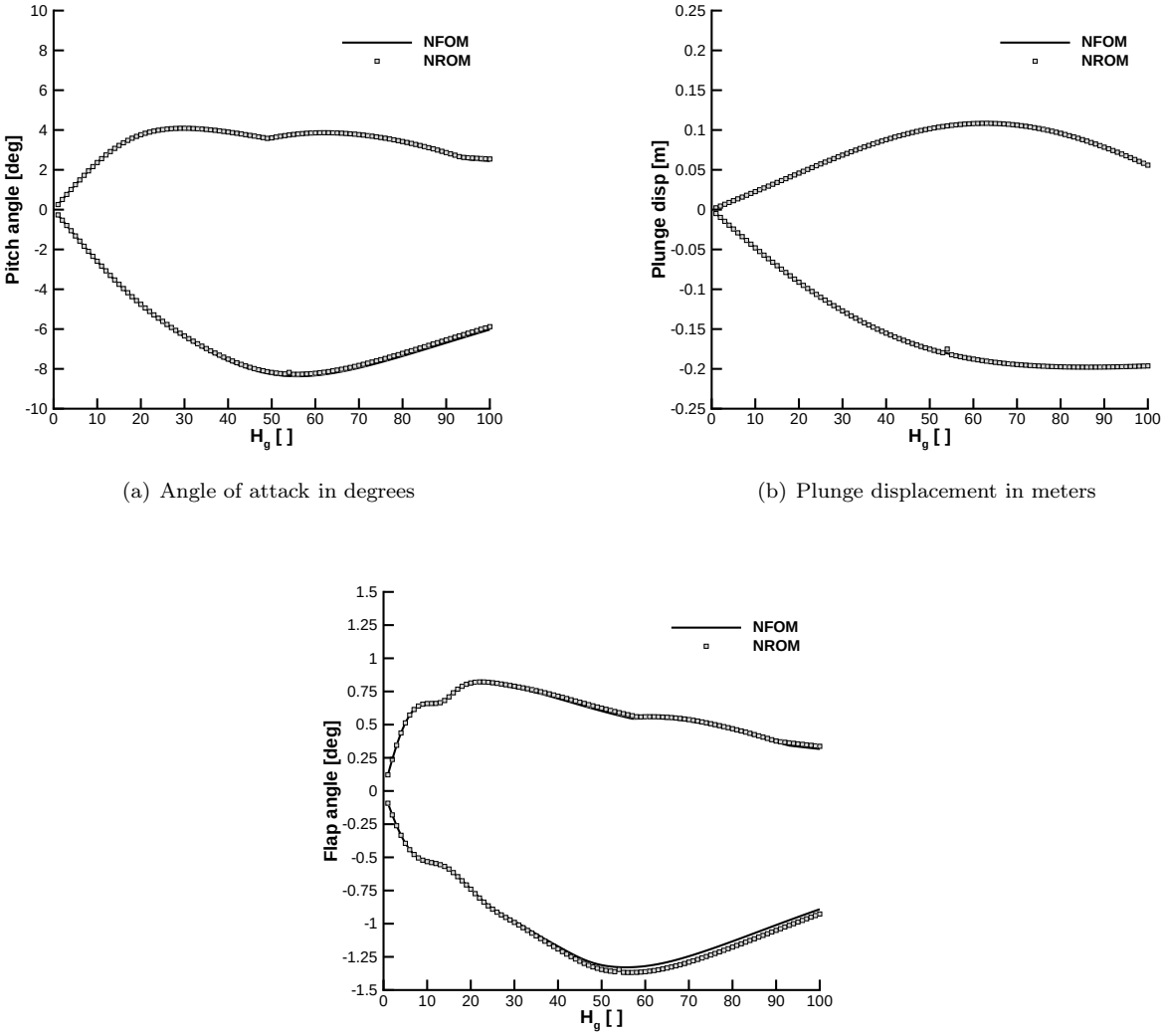

(a) Angle of attack in degrees

(b) Plunge displacement in meters

(c) Flap angle in degrees

Figure 3. Worst-case gust search at $(U^* = 4.5)$ **for 1 minus cosine gust of intensity** $W_0 = 0.14$ **for nonlinear full and reduced model**

It is possible to observe that structural nonlinearity causes larger deformations compared to the linear case. Hence, nonlinearity introduces more criticality.

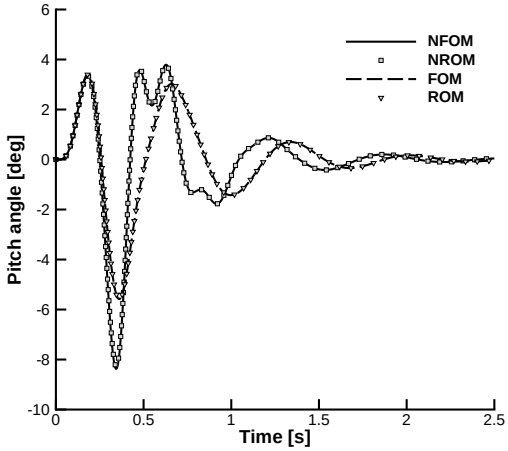

(a) Angle of attack in degrees

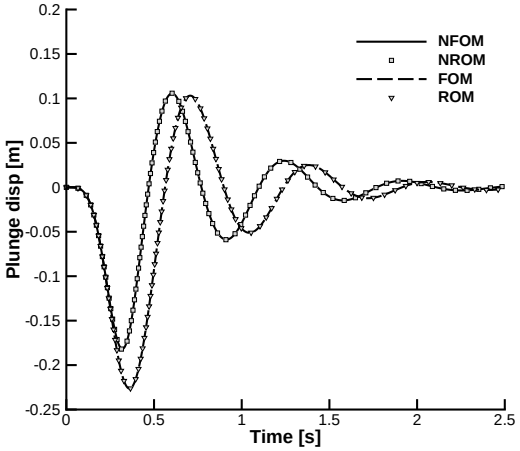

(b) Plunge displacement in meters

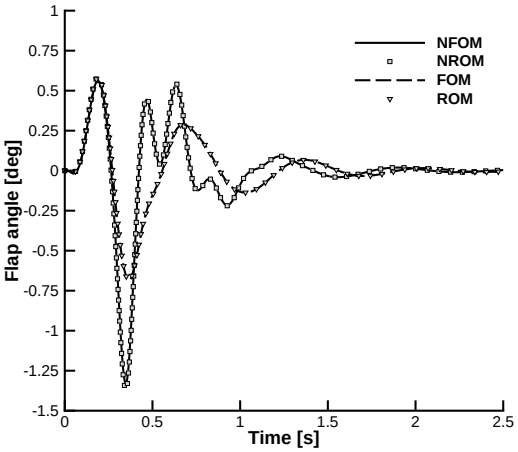

(c) Flap angle in degrees

Figure 4. Aeroelastic response at $(U^* = 4.5)$ for the worst "1-minus-cosine" gust of intensity $W_0 = 0.14$ for nonlinear full against linear and the reduced models

3. *Adaptive Gust Load Alleviation*

The control design for the worst-case gust is done using the model reference adaptive controller. The eigenvalues of the nonlinear reduced order model and that of the reference model are given in Table 2. There is not any specific rule to choose a reference model. However, it is desired the reference model to have more damping and thus being more robust under disturbances. Apart from damping, the first bending frequency is placed far from the first torsional mode frequency which also results in an increase of the flutter speed.[4] Table 2 shows that aeroelastic modes are more damped while their frequencies have been kept apart. The model is dimensionalised by choosing a semi-chord of $b = 0.175$ m and $\omega_\xi = 22.9441$ rad/s.

Table 2. Nondimensional Reduced and Referece Model eigenvalues

ROM	Reference
-0.0407 + 0.2098i	-0.1444 + 2.2748i
-0.0407 - 0.2098i	-0.1444 - 2.2748i
-0.01826 + 0.8588i	-0.0716 + 7.7368i
-0.01826 - 0.8588i	-0.0716 - 7.7368i
-0.01324 + 0.0583i	-0.0360 + 0.4635i
-0.01324 - 0.0583i	-0.0360 - 0.4635i
-0.1393	-0.1393
-0.1393	-0.1393

The model reference control design was based on a particular selection of a positive semi definite matrix $\boldsymbol{Q}$ and additional tuning of the control matrix $\boldsymbol{\Gamma}$. Matrix $\boldsymbol{Q}$ was defined as a diagonal matrix with positive elements $(Q_{11} = 10, Q_{22} = 10, Q_{33} = 30, Q_{44} = 30, Q_{55} = 30, Q_{66} = 10, Q_{77} = 30, Q_{88} = 30)$. The selection of that matrix will provide a solution to the Lyapunov equation in Eq. (30) which is a static parameter in the adaptation of the control law. The design also depends in the selection of the matrix $\boldsymbol{\Gamma}$ as in Eq. (34). In this case for simplicity and in order to demonstrate the effect of that selection on the closed-loop performance the above matrix was scaled by matrix $\boldsymbol{Q}$ and three cases were examined for $(\boldsymbol{\Gamma} = 0.1\boldsymbol{Q}, \boldsymbol{\Gamma} = 0.5\boldsymbol{Q}, \boldsymbol{\Gamma} = 1\boldsymbol{Q})$.

The adaptive controller in general is not expected to be optimal under unknown disturbances due to the fact that the disturbance vector is considered unknown and is not used in the calculation of the controller compared to other designs such as $\boldsymbol{H}_\infty$. Regardless, in Fig. 5 for the angle of attack of the closed-loop system, there is initial overshooting at larger adaptation rates but the oscillations decay to zero faster. For the plunge degree-of-freedom the controller provided overall better response. As expected, the flap angle is affected by the adaptation rate as well. For a larger adaptation rate the flap angle became larger during the structure-gust interaction. As a result, a very large adaptation rate may lead to an urealistic flap actuation either in frequency or rotation which can result in an initial overshooting that can cause structural failure. Thus, should be addressed carefully.

Futhermore, for the plunging degree-of-freedom it is shown that by increasing the adaptation rate there is a reduction in the loads. However, for the pitching degree-of-freedom this is the case for $\boldsymbol{\Gamma} = 0.5\boldsymbol{Q}$ but a further increase causes an overshooting which affects the overall performance of the closed-loop system. A desired choice would be to minimize the loads in both the pitching and the plunging and at the same time keeping the maximum closed-loop angle of attack smaller than the open loop maximum. Also, it should be noted that for a smaller selection of the semi definite positive matrix $\boldsymbol{Q}$ the range of selection of matrix $\boldsymbol{\Gamma}$ would have been broader and this is attributed to the fact that the overall derivative of the adaptation law is affected by the magnitude of the above selections as shown in Eq. (34).

B. Global Hawk-like Flexible Aircraft

1. *Validation*

The aeroelastic code used here has been validated for gust responses against the commercial aeroelastic software NASTRAN. Also, the strip theory assumption for incompressible flow has been tested for gust responses up to 0.3 Mach number against the CFD solver developed at the University of Liverpool.[31]

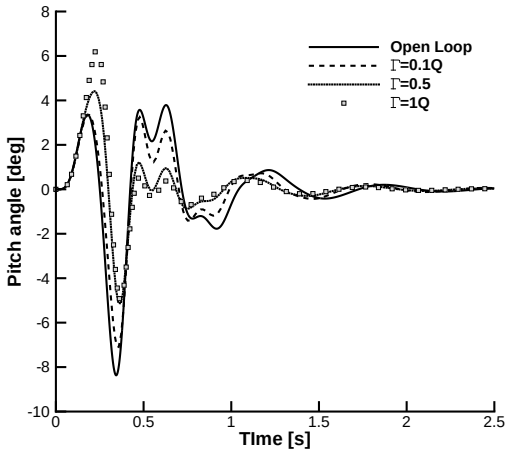

(a) Angle of attack in degrees

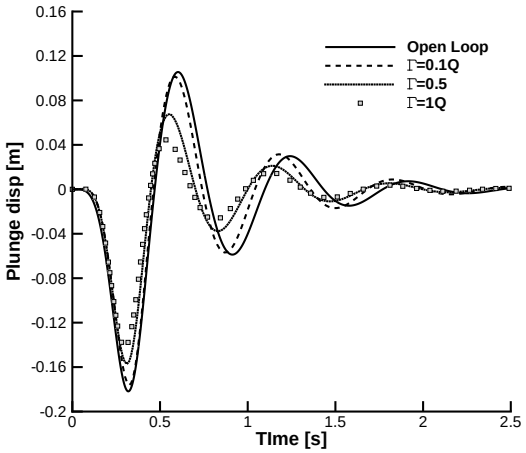

(b) Plunge displacement in meters

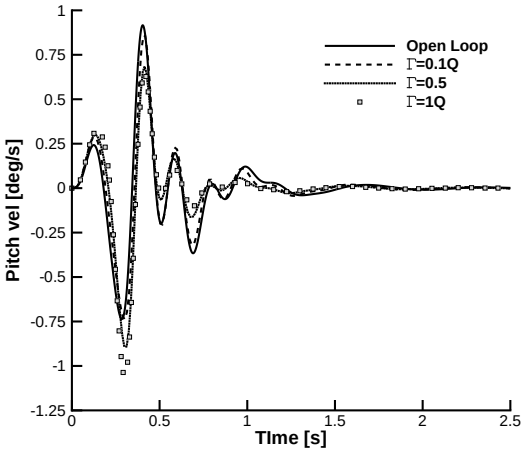

(c) Pitch Velocity in degrees/sec

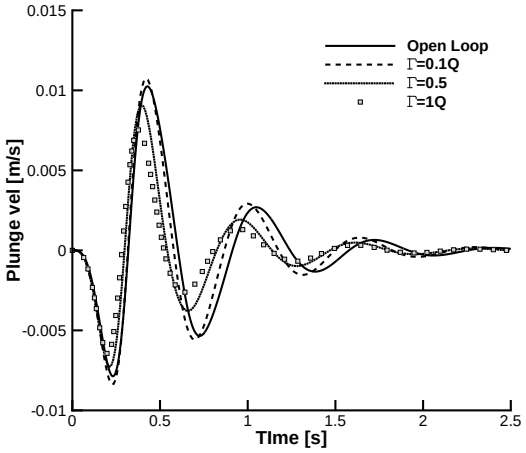

(d) Plunge Velocity in meters/sec

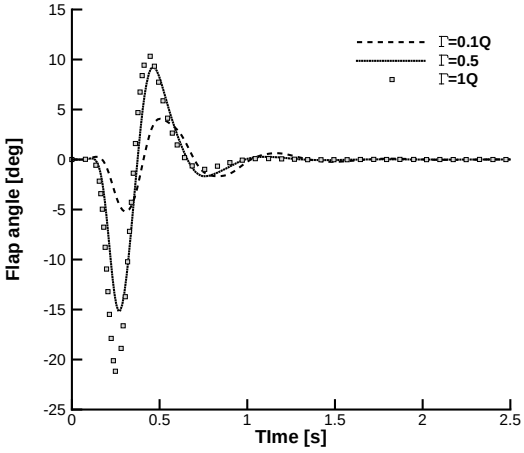

(e) Flap angle in degrees

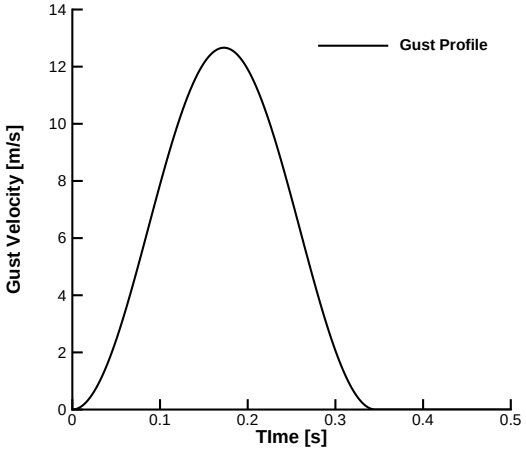

(f) Worst Case Gust Profile

Figure 5. Closed loop response predictions from nonlinear reduced order model for different adaptation rates at ($U^* = 4.5$)

2. Nonlinear Model Reduction

The test case under investigation is an unmanned aerial vehicle (UAV), as shown in Fig. 6. Originally it was a model produced by DSTL for reasearch purposes. The structural model consists of high-aspect ratio wings, a fuselage and a V-tail. For control purposes, trailing-edge control surfaces are placed across the wings and tail. The structural mass of the aircraft is 4732.5 Kg, with the centre of gravity placed at 6.382 m from the nose of the aircraft. The fuel loads in the wing box were modelled with non-structural masses. The front and rear spars are located at 15 and 77% of the local chord of the wing, and at 15 and 80% of the local chord of the V-tail. Additional geometric characteristics are shown in Table 3

Table 3. Unmmaned aerial vehicle geometrical characteristics

Parameter	Wing [m]	Tail [m]
Span	17.71	3.23
Root chord	1.66	1.393
Tip chord	0.733	0.678

A fairly large aeroelastic model is built for the full order model consisting of 540 degrees of freedom that follows the formulation described in section 2. Only half model configuration is considered due to the symmetry of the problem. Control surfaces are mounted on both main wing and canted tail to provide longitudinal control and trim characteristics. Furthermore, they are placed between the $37\% - 77\%$ of the wing span and tail, having a 32% of the average chord length. The beam model used here was derived from

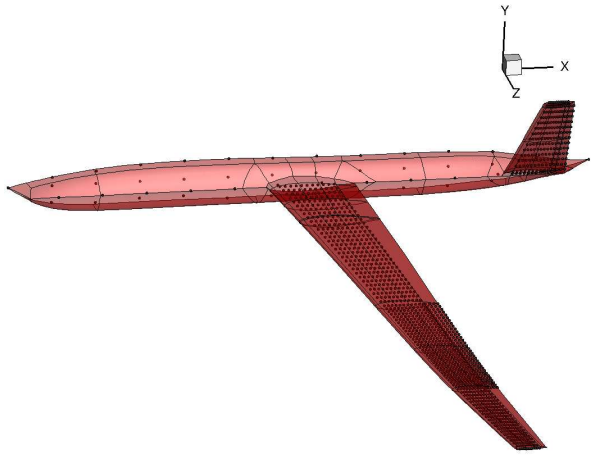

Figure 6. Geometry of a UAV configuration

a detailed structural model. Then it was verified against ground vibration tests and was found adequate to represent the frequencies and shapes of the natural modes of interest. A more detailed description of the above problem was presented in.[3] The reduced models are able to capture nonlinear flexiblity effects for wings exhibiting large structural deformations during a fluid–structure and gust interaction. A 1-cos gust was assumed at the flow conditions given in Table 4. The rational approximation documented in [30] can be used for the generation of continuous models of atmospheric Von Kármán turbulence.

For the flow conditions given in Table 4, the nonlinear static deformation brought the wing tip vertical deflection at 2.2m. With a wing semi–span of 17.71m, the static aeroleastic deformations are relatively large (e.g. 12.5% of the wing span). Two reduced models were generated at this flight condition. One model represents the linearized aeroelastic system, and the other one includes the nonlinear terms up to second order. Both models were build using 11 modes for the projection. Since for a slender wing the coupling between flexural and torsional modes is low, the two lowest bending and the first torsional modes were included. Aerodynamics–dominated modes (related to gust disturbance) were then included until

Table 4. Flow conditions and gust properties

Altitude	20.000 m
Freestream speed U_∞	0.2×295.0 m/s
Density ρ_∞	0.0785 kg/m^3
Angle of attack AoA	2.0 degrees

convergence as in Table 5. The convergence of the reduced model predictions to a "1-minus-cosine" gust for

Table 5. Reduced order model basis

Type	Real	Imaginary
Structural	-15.7545	14.9556i
Structural	-7.9321	31.7767i
Structural	-0.1313	32.9253i
Aerodynamic	-1.1724	0
Aerodynamic	-5.5824	0
Aerodynamic	-5.7598	0
Aerodynamic	-5.8980	0
Aerodynamic	-6.0111	0
Aerodynamic	-6.3911	0
Aerodynamic	-6.6017	0
Aerodynamic	-6.8199	0

increasing number of eigenvectors is shown in Fig. 7. The first bending and torsional modes together with a few dominant aerodynamic modes corresponding to the Küssner gust term are sufficient to obtain identical to the full model response. In this case a reduction from 540 degrees of freedom to 11 was achieved.

Figure 8 illustrates the time response of the UAV wing tip vertical displacement for two sets of results for a shorter gust length with the same reduced models. The first set of data represents the system response when nonlinear flexibility effects are neglected. The linear reduced model is identical to the linearized full order model. The second set of results includes the nonlinear flexibility effects in both reduced and full models. Whereas deformations are very large (10m for a 17.75m wing span), the nonlinear reduced model is virtually identical to the reference solution.

In Fig. 9 the ability of the reduced models to predict aeroelastic responses under stochastic turbulence by Von Kármán is demonstrated showing that one ROM can be used systematically for parametric search being independent of the gust.

3. Adaptive Gust Load Alleviation

The nonlinear reduced model was implemented to simplify and speed up the calculation of an adaptive model reference control framework. The resulted control surface deflection was applied on the nonlinear full order model which is under external disturbances. The selection of the reference model is of critical importance as a bad choice could potentially lead the flap to experience unrealistic rotations. In this case the reference was selected in the same way as it was described in section 3. Damping is added to the first bending mode while the torsional frequencies are kept apart from the bending frequency. The eigenvalues of the linearised reference model are given in Table 6. A direct comparison for the wing tip response of the reference against the nonlinear full order model for the two cases of gusts used in this study is shown in Fig. 10.

The selection of the semi definite positive matrix $\boldsymbol{Q}$ which provides a solution to the Lyapunov equation given a stable Hurwitz matrix of a reference model $\boldsymbol{A_m}$ is also critical. In this case, $\boldsymbol{Q}$ was chosen to be a diagonal matrix with elements $Q_{ii} = 10^{-4}$. As shown in Eq. (34) the selection of the reference model will affect how $\boldsymbol{e}(t)$ will evolve during the time integration which is part of the adaptation parameter.

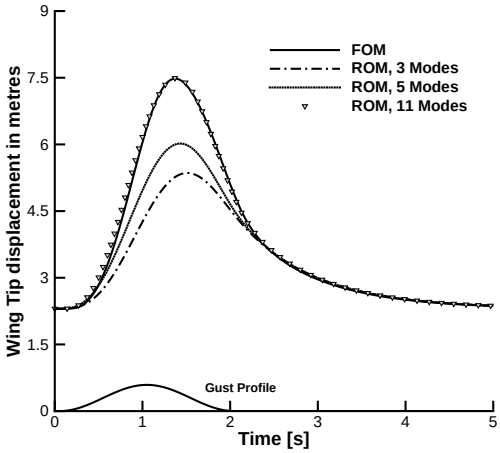

Figure 7. Wing Tip Deformation in metres for a 1 minus cosine gust of intensity 1% of the freestream speed for increasing number of modes for the flow conditions given in Table. 4

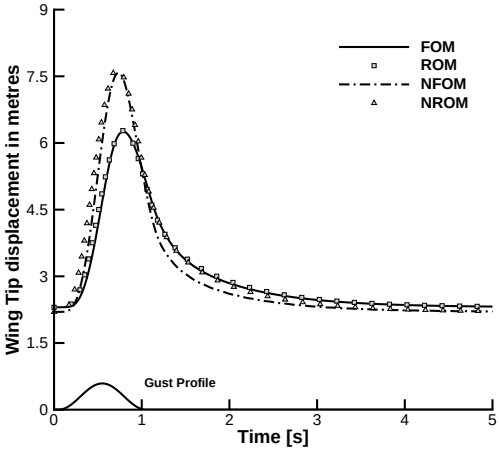

Figure 8. Wing Tip Deformation in metres for 1 minus cosine gust of intensity 1% of the freestream speed for full and reduced models for the flow conditions give in Table. 4

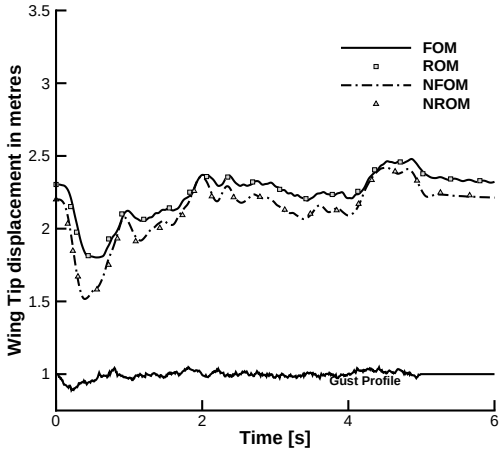

Figure 9. Wing Tip Deformation in metres for stochastic turbulence for full and reduced models for the flow conditions given in Table 4

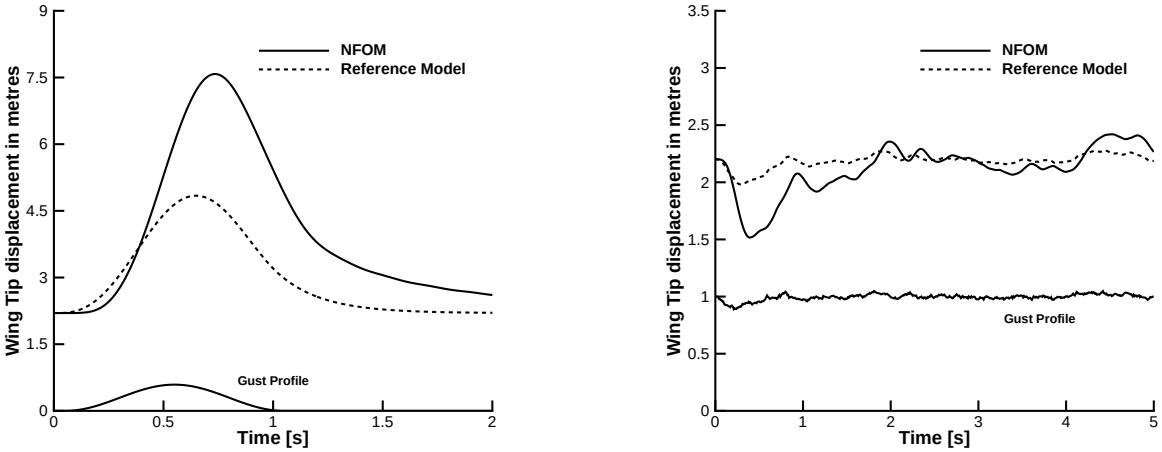

(a) Wing Tip Deformation in metres

(b) Wing Tip Deformation in metres

Figure 10. Wing Tip Deformation for 1 minus cosine and a continuous gust for full open loop against the reference model selection

Table 6. Eigenvalues of the reference model

Real	Imaginary
-35.7545	7.9556i
-7.9321	40.7767i
-5.1313	50.9253i
-3.1724	0
-7.5824	0
-10.7598	0
-10.8980	0
-12.0111	0
-12.3911	0
-12.6017	0
-12.8199	0

The reference model in that case needs to be stable so that the error decreases asymptotically. Also, the adaptation parameter is furthermore affected by $\boldsymbol{P}$ and as a result by matrix $\boldsymbol{Q}$ and $\boldsymbol{\Gamma}$.

The effect of the adaptation matrix $\boldsymbol{\Gamma}$ is therefore investigated for the performance of the closed-loop system. The discrete selection of the semi definite positive matrix $\boldsymbol{\Gamma}$ is shown in table 7 for both discrete and continuous gust loads allevation. The derived controller based on the nonlinear reduced model is di-

Table 7. Adaptation matrix selection as a function of $\boldsymbol{Q}$

	Discrete Gust case	Continuous Gust case
$\boldsymbol{\Gamma}$	$0.01\boldsymbol{Q}$	$0.01\boldsymbol{Q}$
$\boldsymbol{\Gamma}$	$0.03\boldsymbol{Q}$	$0.1\boldsymbol{Q}$
$\boldsymbol{\Gamma}$	$1\boldsymbol{Q}$	$1\boldsymbol{Q}$

rectly applied on the full order nonlinear aeroelastic system. The wing tip vertical deformation for different adaptation rates for a deterministic 1 minus cosine gust is shown if Fig. 11.

In that case the effect of the control adaptation rate on the flap rotation is shown in Fig. 11. Note that for a large adaptation rate $\boldsymbol{\Gamma} = 1\boldsymbol{Q}$, a non-realistic flap rotation occurs with a flap angle of over 20 degrees which is the most common constraint of the flap's maximum rotation. As a result, it is dangerous to choose very large adaptation rates because the flap might overshoot during the aeroelastic/gust interaction. The model reference adaptive controller can also be applied in the presence of stochastic atmospheric turbulence. In Fig. 12 the wing tip displacement together with the closed-loop flap rotation are given for a Von Kármán stochastic gust.

Results show significant reduction of the wing tip deformation for the closed-loop system in both linear and nonlinear case and could be achieved under realistic flap deflections. Also, results are in agreement with the 3 degrees-of-freedom aerofoil model as it can be seen that for the particular selection of the semi-definite positive matrix $\boldsymbol{Q}$ a larger adaptation gain $\boldsymbol{\Gamma}$ is required during the fluid-structure and gust interaction to alleviate the disturbances. A further increase though of the adaptation gain may lead in additional numerical problems due to the fact that the system becomes stiff and it may produce numerical inconsistencies together with the need for a smaller timestep integration but as well as unrealistic flap rotation.

VI. Conclusions

This investigation presents a detailed aeroelastic model of a three degrees-of-freedom aerofoil and couples a nonlinear structural beam code with linear potential aerodynamics sufficient to describe low speed aeroelastic responses. It focuses on the generation of nonlinear reduced models able to be used for a cheaper computation

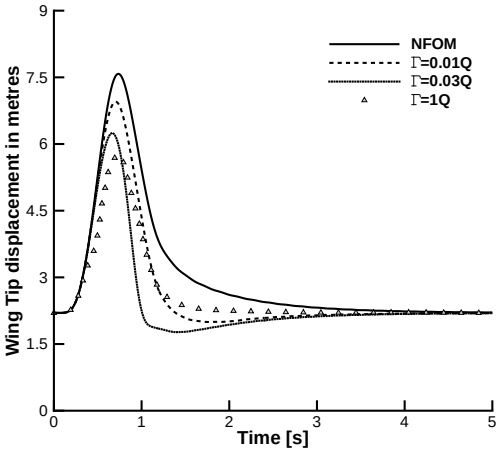

(a) Wing Tip Deformation in metres

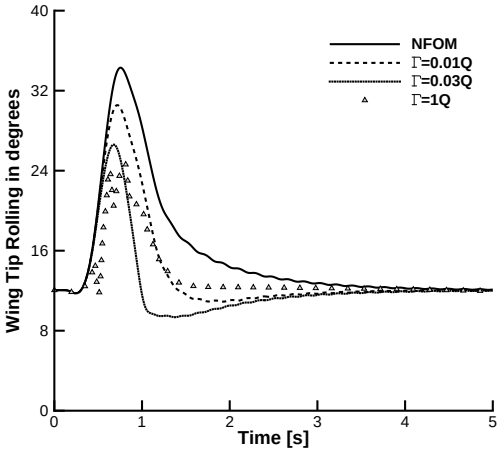

(b) Wing Tip Rolling in degrees

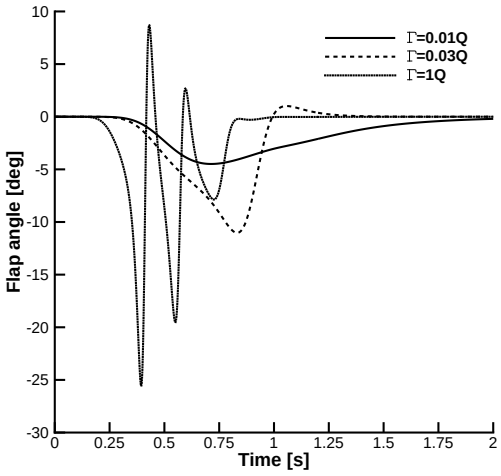

(c) Flap Rotation under different adaptation rates in degrees for a deterministic 1 minus cosine gust

Figure 11. Wing tip deformation and wing tip rolling for 1 minus cosine gust of intensity 1% of the freestream speed for full open loop against closed-loop for different adaptation rates

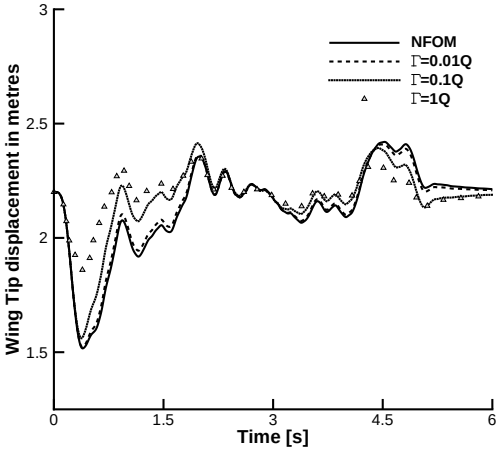

(a) Wing Tip Deformation in meters

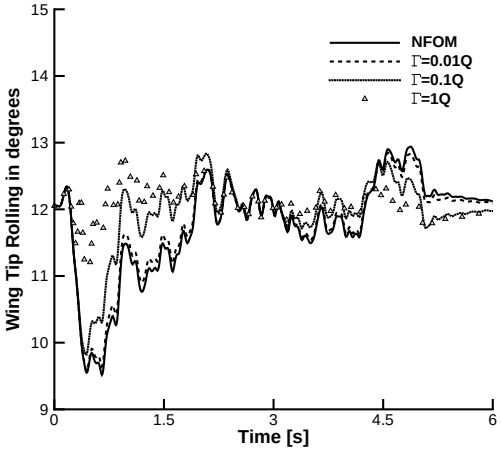

(b) Wing Tip Rolling in degrees

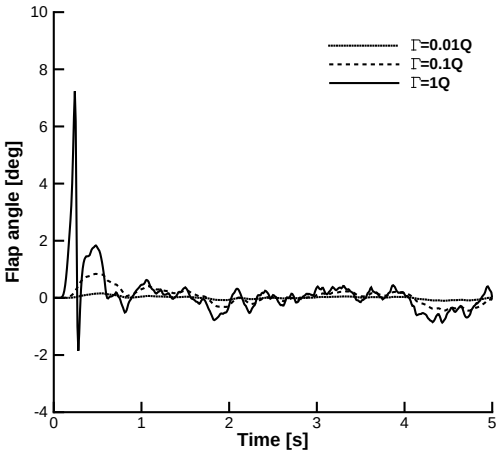

(c) Flap deflection under different adaptation rates in degrees for a stochastic gust

Figure 12. Wing tip deformation and wing tip rolling in for stochastic turbulence for full open loop against closed-loop for different adaptation rates

of an adaptive controller based on the model reference adaptive control scheme and also for a cheaper solution of open loop gust predictions for nonlinear aeroelastic systems. It presents the synthesis, design, and testing of the control strategy developed around the nonlinear reduced order model for gust loads alleviation and this is shown to be systematic because it is independent of the original equations. As expected in both cases, the selection of the adaptation law is critical when dealing with flexible aircraft flight systems. A sufficient enough adaptation rate is needed during the disturbance interaction to regulate the system under deterministic and stochastic disturbances.

Acknowledgements

NDT,GG and KJB, wish to acknowledge the support of the U.K. Engineering and Physical Sciences Research Council (EPSRC) grant EP/I014594/1 on Nonlinear Flexibility Effects on Flight Dynamics and Control of Next–Generation Aircraft. Furthermore, the first author is also gratefull to H. Hesse and Y. Wang for their help with the nonlinear beam code.

References

[1]Da Ronch, A., Badcock, K. J., Wang, Y., Wynn, A., and Palacios, R. N., "Nonlinear Model Reduction for Flexible Aircraft Control Design," *AIAA Atmospheric Flight Mechanics Conference*, AIAA Paper 2012–4404, Minneapolis, MN, 13–16 August 2012, doi: 10.2514/6.2012–4404.

[2]Da Ronch, A., Tantaroudas, N. D., Timme, S., and Badcock, K. J., "Model Reduction for Linear and Nonlinear Gust Loads Analysis," *54th AIAA/ASME/ASCE/AHS/ASC Structures, Structural Dynamics, and Materials Conference*, AIAA Paper 2013–1492, Boston, MA, 8–11 April 2013, doi: 10.2514/6.2013–1492.

[3]Da Ronch, A., Tantaroudas, N. D., and Badcock, K. J., "Reduction of Nonlinear Models for Control Applications," *54th AIAA/ASME/ASCE/AHS/ASC Structures, Structural Dynamics, and Materials Conference*, AIAA Paper 2013–1491, Boston, MA, 8–11 April 2013, doi: 10.2514/6.2013–1491.

[4]Papatheou, E., Tantaroudas, N. D., Da Ronch, A., Cooper, J. E., and Mottershead, J. E., "Active Control for Flutter Suppression: an Experimental Investigation," *International Forum on Aeroelasticity and Structural Dynamics*, IFASD Paper 2013–8D, Bristol, U.K., 24–27 June 2013.

[5]Cook, R. G., Palacios, R., and Goulart, P., "Robust Gust Alleviation and Stabilization of Very Flexible Aircraft," *AIAA Journal*, Vol. 51, No. 2, February 2013.

[6]Strganac, T. W., Ko, J., Thompson, D. E., and Kurdila, A. J., "Identification and Control of Limit Cycle Oscillations in Aeroelastic Systems," *Journal of Guidance, Control, and Dynamics*, Vol. 23, No. 6, 2000, pp. 1127–1133.

[7]Da Ronch, A., Tantaroudas, N. D., Jiffri, S., and Mottershead, J. E., "A Nonlinear Controller for Flutter Suppression: from Simulation to Wind Tunnel Testing," *AIAA SciTech 2014, 55th AIAA/ASMe/ASCE/AHS/SC Structures, Structural Dynamics, and Materials Conference*, AIAA Paper 2014–0345, National Harbor, MD, 11–15 January 2014, doi:10.2514/6.2014–0345.

[8]Rui, H., Haiyan, H., and Yonghui, Z., "Designing active flutter suppression for high-dimensional aeroelastic systems involving a control delay," *Journal of Fluids and Structures*, Vol. 34, 2012, pp. 33–50.

[9]Dillsaver, M. J., Cesnik, C. E. S., and Kolmanovsky, I. V., "Gust Load Alleviation Control for Very Flexible Aircraft," *AIAA Atmospheric Flight Mechanics Conference*, AIAA Paper 2011–6368, 2011.

[10]Gibson, T. E., Annaswamy, A. M., and Lavretsky, E., "Modeling for Control of Very Flexible Aircraft," *AIAA Guidance, Navigation, and Control Conference*, AIAA Paper 2011–6202, 2011.

[11]Cao, C. and Hovakimyan, N., "Adaptive control for nonlinear systems in the presence of unmodelled dynamics:part II," *Proceedings of the American Control Conference,Seattle,WA*, pp. 4099–4104.

[12]Cao, C. and Hovakimyan, N., "L_1 adaptive controller to wing rock," *In:Proceeding of AIAAA Guidance,Navigation and Control Conference AIAA*, 2006-6426 Keystone,CO.

[13]Cao, C. and Hovakimyan, N., "L_1 adaptive output-feedback controller for non-strictly-positive-real reference systems:missile longitudinal autopilot design," *Journal of Guidance,Control,and Dynamics*, Vol. 32, pp. 717–726.

[14]Keum, W. L. and Sahjendra, N. S., "L_1 adaptive control of a nonlinear aeroelastic system despite gust load," *Journal of Vibration and Control*, Vol. 0(0)1-15, 2012.

[15]Ponnusamy, S. and Guibe, J., "Adaptive output feedback control of aircraft flexible modes," *2nd International Conference on Communications Computing and Control Applications,CCCA 2012*, Marseille,France 6 December.

[16]Chowdhary, G., Johnson, E., Kimbrell, M., Chandramohan, R., and Calise, A., "Flight Test Results of Adaptive Controllers in Presence of Severe Structural Damage," *AIAA Guidance,Navigation and Control Conference*, 2010.

[17]Yucelen, T. and Calise, A., "Derivative-Free Model Reference Adaptive Control of a Generic Transport Model," *AIAA Guidance Navigation and Control Conference*, 2 August 2010 through 5 August 2010.

[18]Theodorsen, T., "General Theory of Aerodynamic Instability and the Mechanism of Flutter," NACA Report Nr. 496, 1935.

[19]Jones, R. T., "The Unsteady Lift of a Wing of Finite Aspect Ratio," NACA Report Nr. 681, 1940.

[20]Leishman, J. G., "Unsteady Lift of a Flapped Airfoil by Indicial Concepts," *Journal of Aircraft*, Vol. 31, No. 2, 1994, pp. 288–297.

[21]Hesse, H. and Palacios, R., "Consistent Structural Linearisation in Flexible–body Dynamics with Large Rigid–body Motion." *Computers& Structures*, Vol. 110–111, pp. 1–14.

[22]Wang, Y., Wynn, A., and Palacios, R., "Robust Aeroelastic Control of Very Flexible Wings using Intrisic Models," *54th AIAA/ASME/ASCE/AHS/ASC Structures, Structural Dynamics, and Materials Conference, Boston, Massachusetts*, 08-11 Apr. 2013.

[23]McCracken, A. J., Kennett, D. J., Badcock, K. J., and Da Ronch, A., "Assessment of Tabular Models using CFD," *AIAA Atmospheric Flight Mechanics Conference*, AIAA Paper 2013–4978, Boston, MA, 19–22 August 2013, doi:10.2514/6.2013–4978.

[24]Ioannou, P. A. and Sun, J., "Robust Adaptive Control," *Prentice- Hall*, 1996.

[25]Ogata, K., "Modern Control Engineering," 2010.

[26]Badcock, K. J. and Woodgate, M. A., "Bifurcation Prediction of Large-Order Aeroelastic Models," *AIAA Journal*, Vol. 48, No. 6, 2010, pp. 1037–1046.

[27]Alighanbari, H. and Price, S. J., "The Post-Hopf-Bifurcation Response of an Airfoil in Incompressible Two-Dimensional Flow," *Nonlinear Dynamics*, Vol. 10, No. 4, 1996, pp. 381–400.

[28]Da Ronch, A., Badcock, K. J., Wang, Y., Wynn, A., and Palacios, R., "Nonlinear Model Order Reduction for Flexible Aircraft Control Design," *AIAA Paper 2012-4044*, 2012.

[29]Irani, S., Sarrafzadeh, H., and Amoozgar, M. R., "Bifurcation of a 3-DOF Airfoil with Cubic Structural Nonlinearity," *Chinese Journal of Aeronautics*, Vol. 24, No. 3, 2011, pp. 265–278.

[30]Campbell, C., ""Monte Carlo Turbulence Simulation Using Rational Approximations to von Karman Spectra," *AIAA Journal*, Vol. 24, No. No.1, 1986.

[31]Da Ronch, A., McCracken, A. J., Tantaroudas, N. D., Badcock, K. J., Hesse, H., and Palacios, R., "Assessing the Impact of Aerodynamic Modelling on Manoeuvring Aircraft," *AIAA SciTech 2014, AIAA Atmospheric Flight Mechanics Conference*, AIAA Paper 2014–0732, National Harbor, MD, 11–15 January 2014, doi:10.2514/6.2014–0732.